

## An experimental study on fracture coalescence characteristics of brittle sandstone specimens combined various flaws

Sheng-Qi Yang <sup>\*1,2</sup>

<sup>1</sup> State Key Laboratory for Geomechanics and Deep Underground Engineering, School of Mechanics and Civil Engineering, China University of Mining and Technology, Xuzhou 221116, PR China

<sup>2</sup> Deep Earth Energy Research Laboratory, Department of Civil Engineering, Monash University, Melbourne, Victoria 3800, Australia

(Received September 11, 2014, Revised December 29, 2014, Accepted January 05, 2015)

**Abstract.** This research aims to analyze the fracture coalescence characteristics of brittle sandstone specimen ( $80 \times 160 \times 30$  mm in size) containing various flaws (a single fissure, double squares and combined flaws). Using a rock mechanics servo-controlled testing system, the strength and deformation behaviours of sandstone specimen containing various flaws are experimentally investigated. The results show that the crack initiation stress, uniaxial compressive strength and peak axial strain of specimen containing a single fissure are all higher than those containing double squares, while which are higher than those containing combined flaws. For sandstone specimen containing combined flaws, the uniaxial compressive strength of sandstone increase as fissure angle ( $\alpha$ ) increases from  $30^\circ$  to  $90^\circ$ , which indicates that the specimens with steeper fissure angles can support higher axial capacity for  $\alpha$  greater than  $30^\circ$ . In the entire deformation process of flawed sandstone specimen, crack evolution process is discussed detailed using photographic monitoring technique. For the specimen containing a single fissure, tensile wing cracks are first initiated at the upper and under tips of fissure, and anti-tensile cracks and far-field cracks are also observed in the deformation process; moreover anti-tensile cracks usually accompanies with tensile wing cracks. For the specimen containing double squares, tensile cracks are usually initiated from the top and bottom edge of two squares along the direction of axial stress, and in the process of final unstable failure, more vertical splitting failures are observed in the ligament region. When a single fissure and double squares are formed together into combined flaws, the crack coalescence between the fissure tips and double squares plays a significant role for ultimate failure of the specimen containing combined flaws.

**Keywords:** brittle sandstone; experiment; combined flaws; crack coalescence; strength

### 1. Introduction

Rock is the fra a kind of natural geological material, which usually consists of unequal flaws with different shapes (such as holes, fissures, inclusions) (Debecker and Vervoort 2009, Feng *et al.* 2009, Hall *et al.* 2006, Janeiro and Einstein 2010, Park and Bobet 2009, Prudencio and Van Sint Jan 2007, Yang and Jing 2011). In order to understand cture mechanism of rock engineering, a lot

---

\*Corresponding author, Professor, E-mail: yangsqi@hotmail.com

of experimental and numerical investigations have been carried out for rocks containing all kinds of different flaws (Lee and Jeon 2011, Li *et al.* 2005, Wong and Einstein 2009, Yang *et al.* 2012, 2013, Yin *et al.* 2014). The previous studies focused mainly on the crack coalescence behavior of pre-cracked rock. In the following, the experimental investigation results for the crack coalescence of flawed rocks will be summarized.

Hall *et al.* (2006) carried out an experimental study on natural and dry specimens of Neapolitan fin-grained tuff, and analyzed the crack coalescence process of specimen containing one and two pre-existing fissures by acoustic emission (AE) and photographic monitoring, which were helpful to predict sudden and unexpected collapses of underground rock engineering. Wong and Einstein (2009) studied experimentally the crack coalescence behavior of Carrara marble specimens containing two parallel pre-existing open fissures, which summarized the influence of the different fissure geometries on the cracking processes. Lee and Jeon (2011) carried out uniaxial compression test for Hwangdeung granite containing a horizontal fissure and an inclined fissure, and analyzed the crack initiation and propagation patterns, which were distinctly different those containing two parallel fissures (Wong and Einstein 2009). Yang and Jing (2011) performed the uniaxial compression experiments for brittle sandstone specimens containing a single fissure, and investigated the effect of fissure length and fissure angle on the strength failure and crack coalescence behavior by photographic monitoring and AE technique. Li *et al.* (2005) made an experimental study on propagation and coalescence of pre-existing cracks in marble specimens under compression, and observed two types of newborn cracks, i.e., tensile wing cracks and secondary shear cracks. Yang *et al.* (2012) made an experimental investigation for brittle sandstone specimens containing three fissures, and characterized the effect of ligament angle on the crack coalescence process and type of brittle sandstone material by photographic monitoring and digital image technique. Based on uniaxial compression experiment results of red sandstone containing two unparallel fissures, Yang *et al.* (2013) investigated the effects of the fissure angle on the strength and deformation behaviors of red sandstone material, and analyzed the real-time crack coalescence process in red sandstone material using photographic monitoring and AE monitoring techniques. Yin *et al.* (2014) studied experimentally the coalescence mechanism between two parallel three-dimensional pre-existing surface cracks in brittle granite specimen under uniaxial compression. The digital speckle correction method (DSCM) was used to analyze the captured images producing strain fields during the cracking process, which revealed the mode of cracking (either tensile, shear or their combination).

However, in real rock engineering practice, some flaws (such as circular hole, square hole or elliptical hole etc.) all existed, which was very possible to coalesce with the pre-existing fissures under complex stress states. Once the coalescence occurs between the holes and the fissures, rock mass will be able to occur the unstable failure. In the previous studies, the fracture coalescence behaviors of some rock material containing the holes or the fissures have been made a lot of investigations from the experimental viewpoint. But less experiments are carried out for real rock specimen containing combined flaws (i.e., the combination of holes and fissures), and the fracture coalescence mechanism of rock material containing combined flaws has not almost been understood. In addition, although there are some limitations, the laboratory experimental tests in small scales still have many advantages. For example, it is easy to control the loading/boundary conditions, and can monitor more data during the failure process of specimen. It is a very important tool to investigate the failure mechanism of rock mass. Therefore, the main aim of this research is to analyze the strength and deformation behaviour of brittle sandstone specimen containing combined flaws, and to investigate its fracture coalescence process.

## 2. Tested material and testing procedure

### 2.1 Tested sandstone material

In order to analyze the fracture coalescence behavior of rock containing pre-existing open flaws, the sandstone material located in Linyi City, Shandong province of China was chosen in this research. The sandstone is a fine-grained heterogeneous material with average unit weight about  $2,650 \text{ kg/m}^3$ . The minerals in the sandstone specimens are mainly feldspar, quartz and detritus, which are the same as tested sandstone material in reference (Yang *et al.* 2012). It is noted that it is very difficult to reproduce all the flawed samples containing combined flaws due to limited samples from the same rock block. Moreover, machining pre-existing flaws especially for very hard rock material is more difficult. However, from the previous experimental studies for the same sandstone material (Yang *et al.* 2012), it is proved that the dispersion of this sandstone material is very small. Therefore, in the current experimental tests, it is believed that the same fracture coalescence mechanism can be studied based on the limited specimens.

### 2.2 Specimens containing pre-existing flaws

In this research, rectangular prismatic specimens of sandstone,  $80 \times 160 \times 30 \text{ mm}$  in size, are prepared to carry out uniaxial compression test. The specimens were machined from a rectangular block along the same direction. The height to width ratios of all the tested specimens are all 2.0, which can ensure a uniform stress state within the central part of the specimens. In order to obtain the exact results as well as the best comparison, all the specimens were carried out in natural and dry conditions.

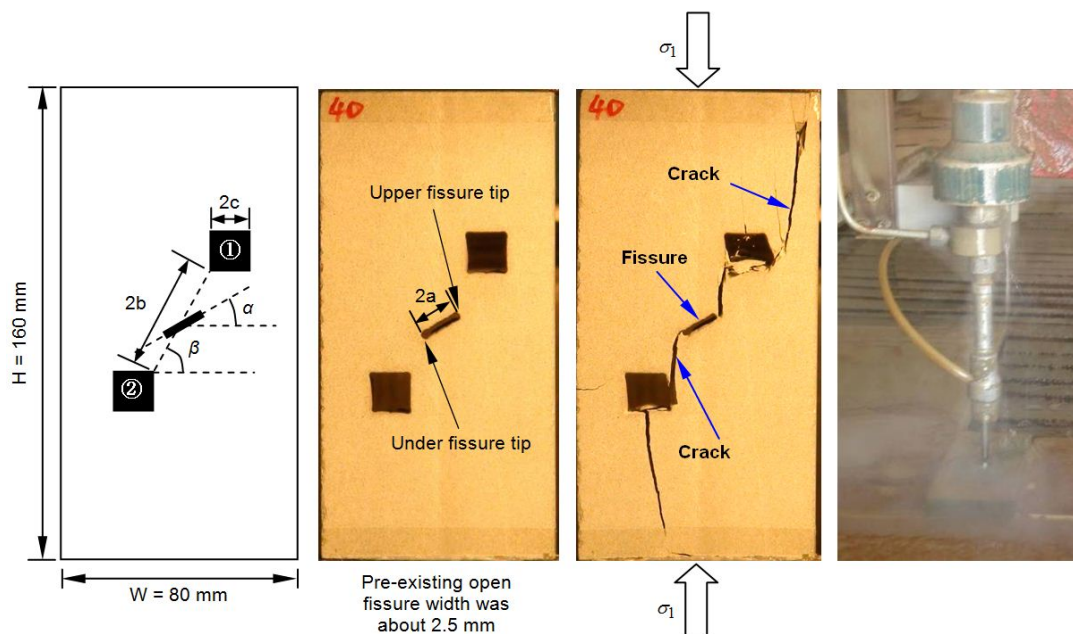


Fig. 1 Geometry of pre-existing sandstone flaws in this research and the flaws were all machined by high pressure water-jet cutting

Table 1 Mechanical parameters of intact and pre-existing flawed sandstone specimens under uniaxial compression

Specimen	$\alpha / ^\circ$	$\beta / ^\circ$	2a /mm	2b /mm	2c /mm	Note	$\varepsilon_{1c}/10^{-3}$	$\sigma_c/\text{MPa}$
B0r <sup>#</sup>	N/A	N/A	N/A	N/A	N/A	Intact specimen	7.051	190.8
B33 <sup>#</sup>	30	N/A	15	N/A	N/A	Single fissure	5.357	140.86
B32r <sup>#</sup>	N/A	60	N/A	40	14	Double squares	4.461	113.37
B40 <sup>#</sup>	30	60	15	40	14	Combined flaws	2.778	43.44
B42 <sup>#</sup>	60	60	15	40	14	Combined flaws	2.539	53.89
B44 <sup>#</sup>	90	60	15	40	14	Combined flaws	3.750	101.92

The geometry of sandstone specimens containing pre-existing flaws is described in Fig. 1, which is different from previous studies (Hall *et al.* 2006, Lee and Jeon 2011, Li *et al.* 2005, Wong and Einstein 2009, Yang *et al.* 2012, Yang and Jing 2011). The geometry of pre-existing flaws is defined by five geometrical parameters - single fissure angle  $\alpha$  (the angle of single fissure with the direction of the horizontal direction), single fissure length 2a, ligament length 2b between two squares ①②, ligament angle  $\beta$  between two squares ①②, square side length 2c.

A high pressure water-jet cutting machine was used to machine combined flaws in intact specimens. Open fissure width was about 2.5 mm. To investigate the effect of pre-existing flaws geometry on the deformation failure and crack coalescence behavior of sandstone under uniaxial compression, different geometries of pre-existing flaws listed in Table 1 were chosen.

### 2.3 Testing procedure

Uniaxial compression tests for intact and flawed sandstone specimens were carried out on a rock mechanics servo-controlled testing system. The axial stress was imposed on the surface of rock specimen until the specimen failed. All the tests were performed under displacement-controlled conditions with a strain rate of  $8.125 \times 10^{-6}/\text{s}$ . In order to decrease the effect of the end friction effects on testing results, two rigid steel blocks ( $33 \times 83 \times 15$  mm) were placed between the loading frame and rock specimen and two antifricition gaskets between two rigid steel blocks and the end surface of specimen (Yang *et al.* 2012).

## 3. Analysis of experimental results

Fig. 2 shows the axial stress-strain curve and ultimate failure mode of intact sandstone specimen under uniaxial compression, and a detailed crack coalescence process has been analyzed in the previous research (Yang *et al.* 2012). In accordance with Fig. 2, it can be seen that the sandstone is very brittle and takes on typically axial splitting failure behavior. In addition, it is noted that the non-linear behavior in the stress-strain curves during the small strain range (up to  $1.5 \times 10^{-3}$ , see Fig. 2) is caused by the closure of some primary cracks, pores and voids in tested sandstone specimen.

### 3.1 Effect of various pre-existing flaws on strength and deformation failure behaviors of sandstone specimens

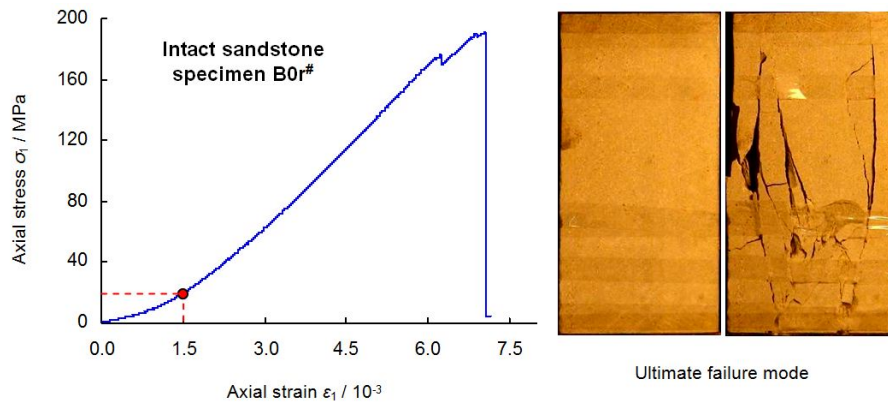


Fig. 2 Axial stress-strain curve and ultimate failure mode of intact sandstone specimen under uniaxial compression (Yang *et al.* 2012)

Fig. 3 shows the entire axial stress-strain curves of flawed sandstone specimens under uniaxial compression, which the corresponding mechanical parameters are listed in Table 1. In Table 1,  $\sigma_c$  is defined as the uniaxial compressive strength and  $\epsilon_{1c}$  refers to peak axial strain. It is noted that the corresponding axial stress initiated the first crack from the tips of fissures is defined as the crack initiation stress, which can be obtained in accordance with the axial stress drop shown in the curves of Fig. 3 when the first crack initiated. It can be obtained by photographic monitoring technique.

Compared with intact specimen as shown in Fig. 2, more stress drops in axial stress-strain curves shown in Fig.3 are observed, which results from some new crack coalescences in flawed sandstone specimens. In accordance with Fig. 3 and Table 1, we can analyze further the influence of various flaws and fissure angles on the strength and deformation behaviors of flawed sandstone specimens.

The intact sandstone specimen has a uniaxial compressive strength of 190.8 MPa, while the peak strength of flawed sandstone specimens ranges from 43.44 MPa (combined flaws,  $\alpha = 30^\circ$  and  $\beta = 60^\circ$ ) to 140.86 MPa (single fissure,  $\alpha = 30^\circ$ ) in this research. However for peak axial strain, the intact sandstone specimen failed at a strain of 0.705% under uniaxial compression, while flawed sandstone specimens failed at a strain of approximately 0.25~0.54%. Therefore, the mechanical parameters of flawed sandstone specimens are all lower than those of intact specimen, but the reduction extent depends on various flaws and fissure angles.

The effect of various flaws on peak strength of flawed sandstone specimens under uniaxial compression is presented in Fig. 4. From Fig. 4, it can be seen that the uniaxial compressive strength of specimen containing a single fissure is 140.86 MPa, which is higher 19.5% than that of specimen containing double squares (113.37 MPa). But the uniaxial compressive strength of specimen containing double squares is higher than that of specimen containing combined flaws. However for sandstone specimen containing combined flaws with two same squares, the uniaxial compressive strength of sandstone is dependent obviously to the fissure angle  $\alpha$ . When  $\alpha$  increases from  $30^\circ$  to  $90^\circ$ , the uniaxial compressive strength increases from 43.44 MPa to 101.92 MPa, which indicates that the specimens with steeper fissure angles can support higher axial capacity for  $\alpha$  greater than  $30^\circ$ . The effect of various flaws on peak axial strain of flawed sandstone specimens under uniaxial compression shows approximately similar behavior as uniaxial compressive

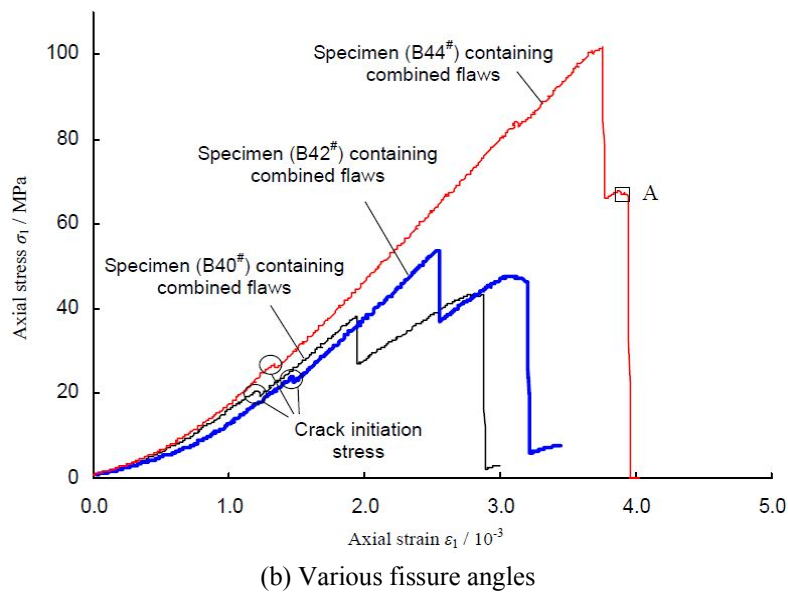
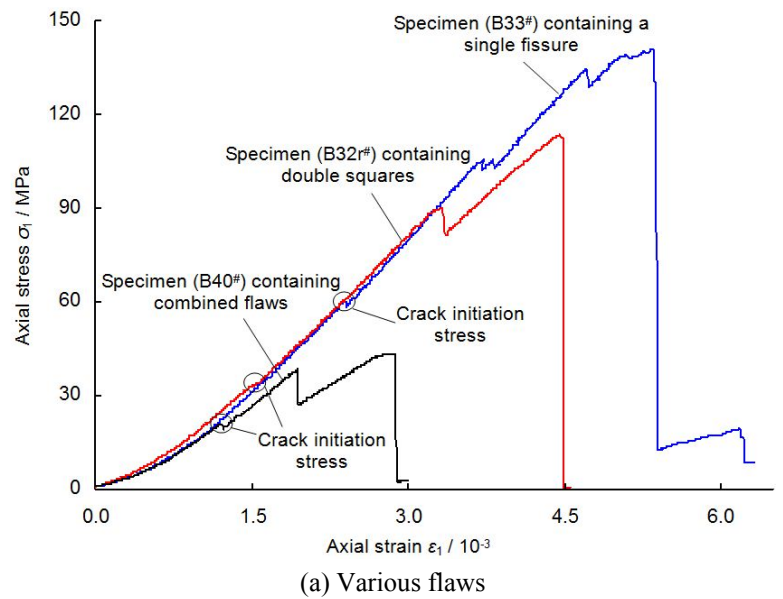


Fig. 3 Axial stress-strain curves of pre-existing flawed sandstone specimens under uniaxial compression

strength.

In Fig. 3, the first stress drops in each flawed specimens are all denoted with the circular point, which means the initiation of the first crack during loading. The corresponding axial stress for the initiation of the first crack is defined as the crack initiation stress in this research. Fig. 4 illustrates the effect of various flaws on crack initiation stress of brittle sandstone specimens under uniaxial compression. From Fig. 4, it is very clear that the crack initiation stresses of brittle sandstone specimens are all lower than the peak strength, but the reduction extent is closely related to

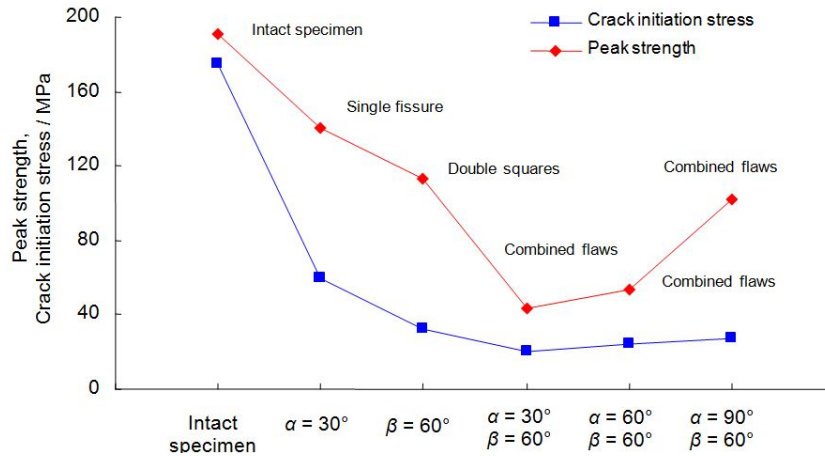


Fig. 4 Effect of various flaws on peak strength and crack initiation stress of brittle sandstone specimens under uniaxial compression

pre-existing flaw geometries. The crack initiation stress of intact specimen reaches 174.5 MPa, which is higher 65.6% than that of specimen containing a single fissure (60.1 MPa). But the crack initiation stress of specimen containing a single fissure is higher 45.5% than that of specimen containing two squares. However for sandstone specimen containing combined flaws with two same squares, as  $\alpha$  increases from  $30^\circ$  to  $90^\circ$ , the crack initiation stress increases from 20.68 MPa to 27 MPa, which indicates that the crack initiation stress of sandstone containing combined flaws is not dependent obviously to the fissure angle.

Fig. 5 presents ultimate failure modes of flawed sandstone specimens under uniaxial compression. It needs to be noticed that the failure mode of specimen containing combined flaws with  $\alpha = 90^\circ, \beta = 60^\circ$  is not an ultimate failure mode, but that at point A shown in Fig. 3(b). After point A, the specimen took place the tilting failure, which was fractured into many small blocks.

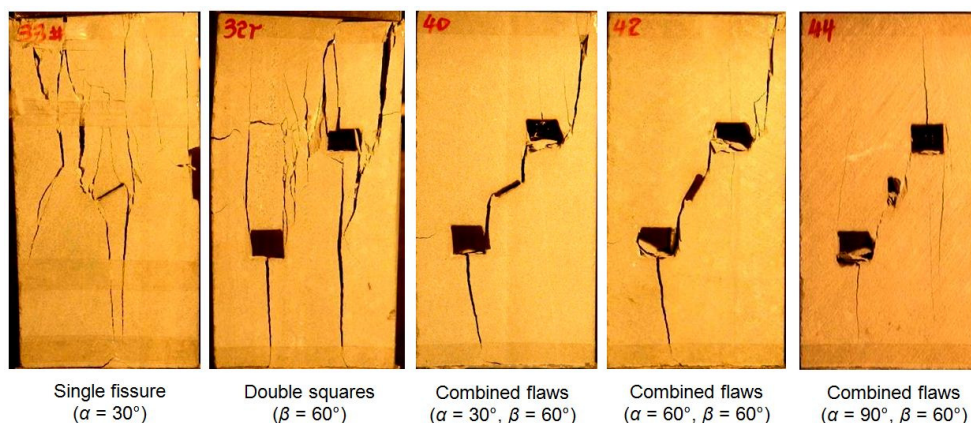


Fig. 5 Ultimate failure modes of flawed sandstone specimens under uniaxial compression. Note that the failure mode of specimen containing combined flaws with  $\alpha = 90^\circ, \beta = 60^\circ$  is that at the point A shown in Fig. 3(b)

From Fig. 5, we can conclude that ultimate failure modes of flawed sandstone specimens depend on various flaws and fissure angles. For the specimen containing a single fissure, the macroscopic failure mode is a mixture of tensile wing crack, anti-tensile crack, secondary tensile crack, and far-field crack (Yang and Jing 2011). For the specimen containing double squares, the macroscopic failure mode is a mixture of many tensile cracks along the direction of axial stress, and due to the interaction of stress field between two squares ①②, more vertical splitting failures occur in the ligament area. But for the specimens containing combined flaws, the macroscopic failure mode are approximate same for  $\alpha = 30^\circ$  and  $60^\circ$ . The two specimens merges between the upper tip of the fissure and the left bottom corner of square ①, and between the under tip of the fissure and the right side of square ②. However for the specimen containing combined flaws with  $\alpha = 90^\circ$ , the coalescence occurs between the under tip of the fissure and the right center side of square ②, and between the under tip of the fissure and the left bottom corner of square ①. Besides, there are a lot of hole collapses in the specimens containing combined flaws compared with the specimen containing double squares. Finally, it should be noticed that the fracture coalescence of all flawed specimens is a gradual evolution process with the increase of axial deformation, which will be made a detailed analysis in the following sections.

### 3.2 Crack evolution behavior of sandstone specimens containing a single fissure and double squares

Fig. 6 shows the axial stress-strain curve and its local magnification of sandstone specimen containing a single fissure ( $\alpha = 30^\circ$ ,  $2a = 15$  mm) under uniaxial compression, and the crack evolution process of sandstone specimen containing a single fissure is also presented in Fig. 7. The denoted letters in Fig. 7 are corresponding to those in Fig. 6.

In accordance with Figs. 6-7, when the specimen is loaded to point a, tensile wing cracks  $1^a$  and  $1^b$  originate from the upper and under tip of fissure, respectively. Notice, the initiation direction of crack 1 is vertical to pre-existing fissure, and then propagates towards the end surface of the specimen along the direction of axial stress. At the stage of ac, with the increase of axial deformation, the width and length of crack 1 all increase (see Fig. 7(b)). When the specimen is

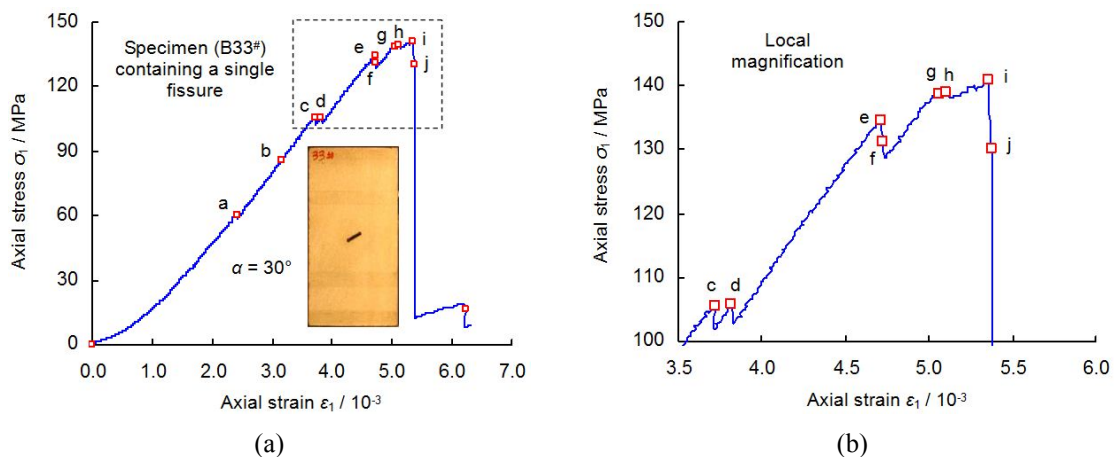


Fig. 6 Axial stress-strain curve and its local magnification of sandstone specimen containing a single fissure ( $\alpha = 30^\circ$ ,  $2a = 15$  mm) under uniaxial compression

loaded up to point c, anti-tensile crack 2 is initiated from the upper tip of fissure, and afterwards when being loaded to point d, another anti-tensile crack 3 is also initiated from the under tip of fissure. The rapid formation of anti-tensile cracks 2-3 all result in a minor stress drop of axial stress-strain curve (see local magnification in Fig. 6). Moreover, due to the opening of cracks 2-3, tensile wing cracks  $1^a$  and  $1^b$  all occur to close.

However with the increase of axial deformation, the axial stress of the specimen begins to increase slowly as an approximately same elastic modulus as that before point c. When being loaded to point e, and tensile crack 4 rapidly comes out (see Fig. 7(e)) along the direction of axial stress. After that, tensile crack 5 is initiated from the right bottom part of the specimen (see Fig. 7(f)), which is an obviously vertical splitting failure. Notice, the initiation of tensile cracks 4-5 leads to a continuous stress drop from 134.55 to 131.08 MPa and then to 128.73 MPa. After the above stress drop, the continuous increasing deformation leads to more stress concentrations nearby the under tip of fissure, which induces a secondary anti-tensile crack 6 (see Fig. 7(g)). In



Fig. 7 Crack evolution process of sandstone specimen containing a single fissure ( $\alpha = 30^\circ$ ,  $2a = 15$  mm) with the increase of deformation. The denoted letters shown in the figure are corresponding to Fig. 6

the process of from point g to peak point i ( $\sigma_1 = 140.86 \text{ MPa} = 100\% \sigma_c$ ), the axial stress does not increase a lot with increasing axial deformation, which results mainly from a slow propagation of crack 6 along the direction of axial stress. Of course due to the heterogeneity of sandstone material, the coalescence path of crack 6 is not very smooth. After peak strength, the axial supporting capacity of the specimen begins to drop from 140.86 to 130.15 MPa (point j), which leads to the formation of far-field cracks 7<sup>a</sup>-7<sup>d</sup>. After point j, the specimen occurs to ultimately unstable failure and the axial stress drops to a lower value.

Fig. 8 shows the axial stress-strain curve and its local magnification of sandstone specimen containing double squares under uniaxial compression, and the crack evolution process of sandstone specimen containing double squares is also presented in Fig. 9. The denoted letters in Fig. 9 are corresponding to those in Fig. 8. It is very clear that the crack evolution behavior of sandstone specimen containing double squares is different from that containing a single fissure.

From Fig. 8, it can be seen that when the specimen is loaded to point a ( $\sigma_1 = 33.38 \text{ MPa} = 29.4\% \sigma_c$ ), four tensile cracks 1<sup>a</sup>-1<sup>d</sup> are initiated from the top and bottom edge of two squares (Fig. 9(a)), respectively. In the process of point a to point e, no new cracks are observed but the length of tensile cracks 1<sup>a</sup>-1<sup>d</sup> increases a lot with the increase of axial deformation (Fig. 9(b)-(d)). However, it should be noted that even though the corners of squares had a higher stress concentration, the initiation of fracture emanated from the sidewall of squares rather than the corners. This is because due to the uniaxial compression, the concentrated tensile stress along the vertical middle line of specimen is much higher than the tensile stress concentration at the corners of squares. This stress distribution is something like the stress field in the Brazilian disk. Certainly, if the dip angle of pre-existed crack is not zero, the initiation of fracture could initiate from the corners of pre-existed crack, where the stress concentration is higher than the sidewall of it. When the axial stress reaches to point e ( $\sigma_1 = 90.18 \text{ MPa} = 79.5\% \sigma_c$ ), tensile crack 2 originates from the left top corner of square ② and propagates towards the top part of the specimen along the direction of axial stress (Fig. 9(e)), which leads to a stress drop from 90.18 to 85.37 MPa.

Afterwards, due to the coalescence of tensile crack 3<sup>a</sup> from the right top corner of square ① and tensile crack 3<sup>b</sup> from the left top corner of square ②, the axial stress continues to drop from 85.37 to 83.44 MPa. At the stress level of 83.44 MPa (point g), tensile crack 4 induces from the

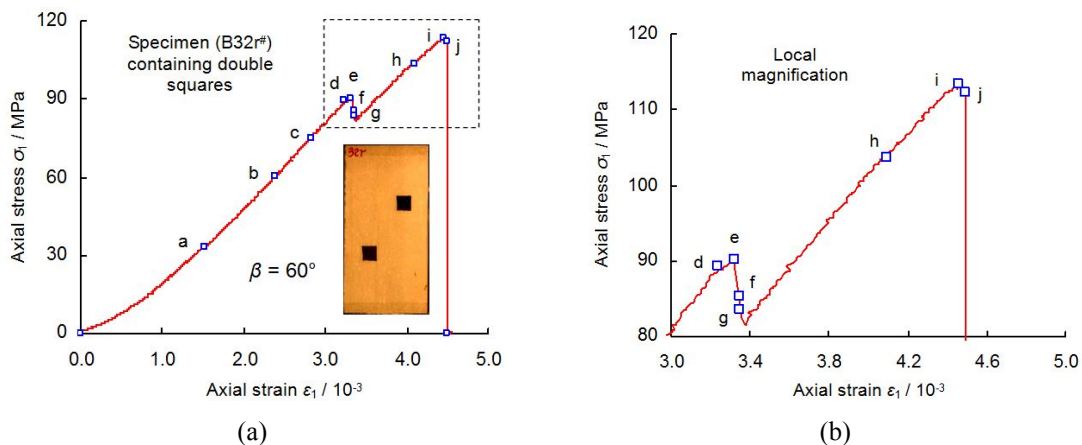


Fig. 8 Axial stress-strain curve and its local magnification of sandstone specimen containing double squares under uniaxial compression



Fig. 9 Crack evolution process of sandstone specimen containing double squares with the increase of deformation. The denoted letters shown in the figure are corresponding to Fig. 8

left bottom corner of square ①, which also results in a minor stress drop from 83.44 to 81.62 MPa. After that, the continuous increase of axial deformation leads to that the specimen is loaded to peak point i, but in this process no new cracks are observed. After peak strength, the axial supporting capacity of the specimen drops to point j, which results from the coalescence of crack 5. After point j, the specimen induces the unstable failure and more vertical splitting failures are observed in the ligament region of the specimen.

### 3.3 Crack evolution behavior of sandstone specimens containing combined flaws

When a single fissure and double squares are combined in the same specimen, the flaw geometry in the specimen becomes the combined flaws. Fig. 10 shows the axial stress-strain curve of sandstone specimen containing combined flaws ( $\alpha = 30^\circ$ ,  $\beta = 60^\circ$ ) under uniaxial compression, and the crack evolution process of sandstone specimen containing combined flaws is also presented in Fig. 11. The denoted letters in Fig. 11 are corresponding to those in Fig. 10. From Figs. 10-11, we can see that the crack evolution process of sandstone specimen containing combined flaws is different from that containing a single fissure and double squares.

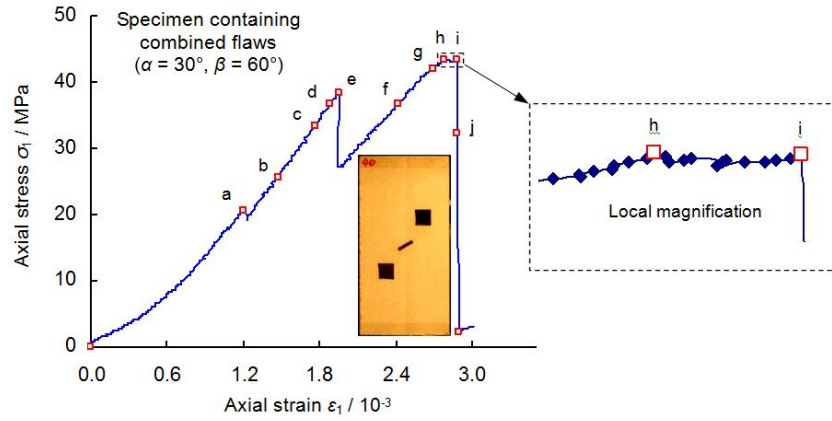


Fig. 10 Axial stress-strain curve and its local magnification of sandstone specimen containing combined flaws ( $\alpha = 30^\circ, \beta = 60^\circ$ ) under uniaxial compression

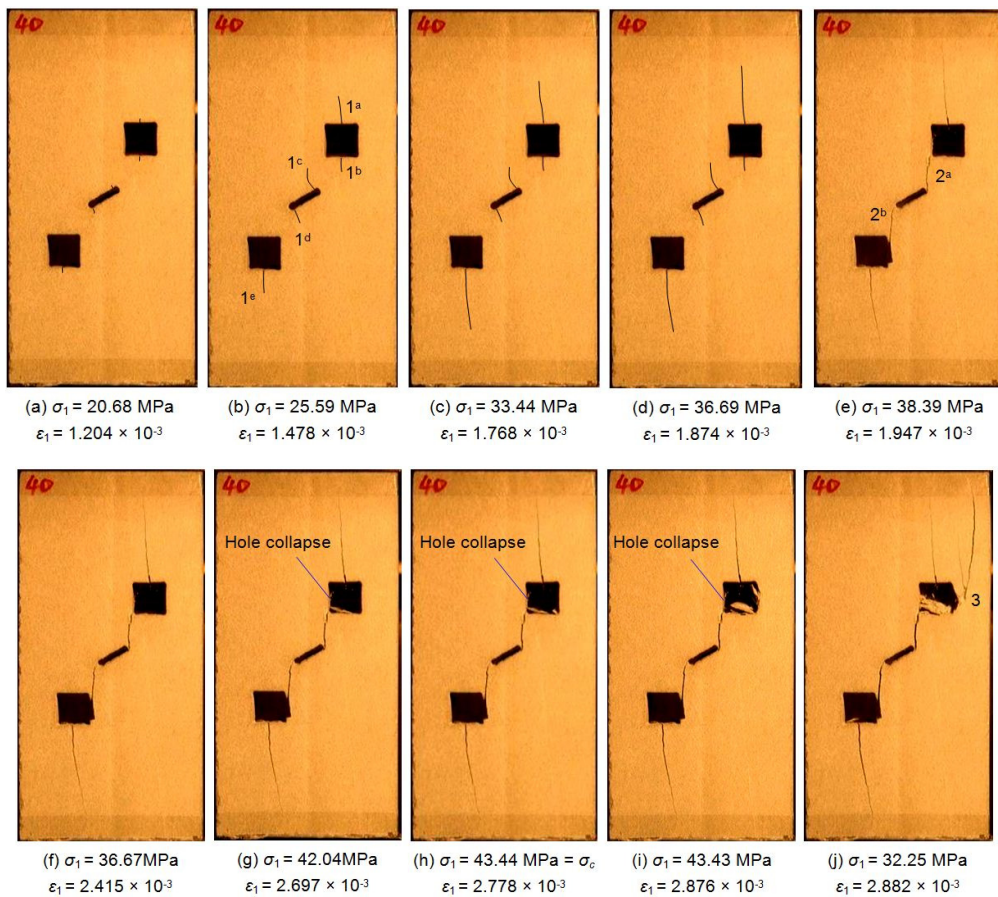


Fig. 11 Crack evolution process of sandstone specimen containing combined flaws ( $\alpha = 30^\circ, \beta = 60^\circ$ ) with the increase of deformation. The denoted letter shown in the figure is corresponding to Fig. 10

In accordance with Figs. 10-11, it is clear that before point a, the stress concentration nearby combined flaws does not reach the material strength to initiate any cracks. While when the axial stress is loaded to point a, the specimen begins to initiate tensile crack 1 at the upper and under tip of fissure, the top and bottom edge of two squares. The initiation of tensile crack 1 leads to that the axial stress drops to 19.24 MPa from 20.68 MPa. After that, with the increase of axial deformation, the length of crack 1 increases a lot especially cracks 1<sup>a</sup> and 1<sup>c</sup>. But it should be noticed that tensile wing cracks 1<sup>c</sup> and 1<sup>d</sup> initiated at the upper and under tip of fissure do not propagate to the end surface of the specimen as that shown in Fig. 7(b), which maybe result from stress concentration field between fissure and double squares. When the specimen is loaded to point e ( $\sigma_1 = 38.39 \text{ MPa} = 88.4\% \sigma_c$ ), tensile crack 2<sup>a</sup> merges rapidly between the upper tip of fissure and the left bottom corner of square ①, and tensile crack 2<sup>b</sup> between the under tip of fissure and the right side part of square ②. The coalescence of tensile crack 2 leads to an obvious stress drop from 38.39 to 27.16 MPa in a smaller range of axial strain.

After the stress drop at point e, the continuous increase of axial deformation leads to that the axial stress of the specimen begins to increase slowly with a lower deformation modulus than that before point e, which results from some minor damages of the supporting structure in the specimen (Fig. 11(e)). When being loaded to point f, the widths of original tensile cracks 1-2 all increase but the lengths do not increase due to the limitation of the edge boundary of the specimen (Fig. 11(f)). When the specimen is loaded to point g, the axial stress-strain curve begins to depart from the linearity because of hole collapse of square ①. Afterwards, the increase of axial deformation leads to that the specimen is loaded to peak point h ( $\sigma_1 = 43.44 \text{ MPa} = 100\% \sigma_c$ ), hole collapse of square ① in the specimen can still be observed. After peak stress, square ① in the specimen comes out more hole collapses (Fig. 11(i)). It should be noticed that in the deformation process from point h to point i, even though the axial strain continues to increase, the axial stress keeps basically a constant, which can be seen from local magnification shown in Fig. 10. Hole collapse of square ① in the specimen is a gradual evolution process, as shown in Fig. 12. After point i, the axial supporting capacity of the specimen drops to point j, which results from the coalescence of crack 3. After point j, the specimen takes place the unstable failure.

When the fissure angle was  $60^\circ$ , the axial stress-strain curve of sandstone specimen containing combined flaws ( $\beta = 60^\circ$ ) under uniaxial compression was shown in Fig. 13 and the corresponding crack evolution process was also presented in Fig. 14. The denoted letters in Fig. 14 corresponded

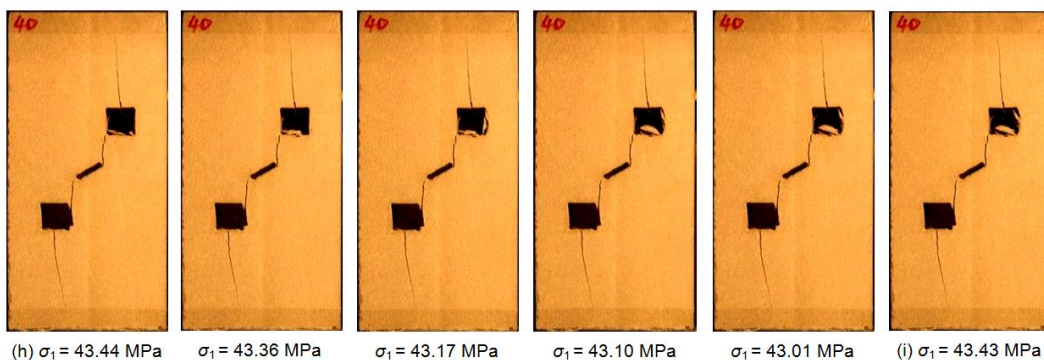


Fig. 12 Gradual evolution process of square hole collapse of sandstone specimen containing combined flaws ( $\alpha = 30^\circ, \beta = 60^\circ$ ) during uniaxial loading. The denoted letter shown in the figure is corresponding to Fig. 10

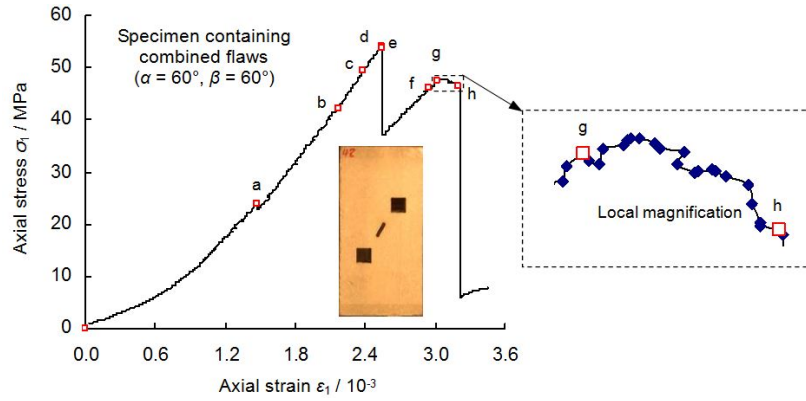


Fig. 13 Axial stress-strain curve and its local magnification of sandstone specimen containing combined flaws ( $\alpha = 60^\circ, \beta = 60^\circ$ ) under uniaxial compression



Fig. 14 Crack evolution process of sandstone specimen containing combined flaws ( $\alpha = 60^\circ, \beta = 60^\circ$ ) with the increase of deformation. The denoted letter shown in the figure is corresponding to Fig. 13

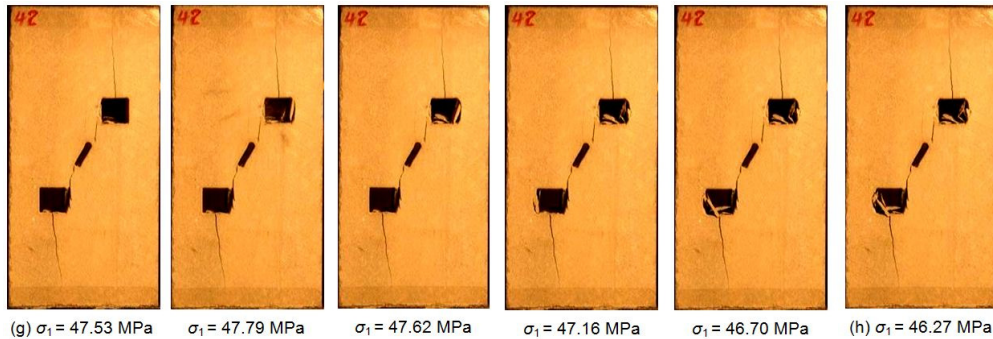


Fig. 15 Gradual evolution process of square hole collapse of sandstone specimen containing combined flaws ( $\alpha = 60^\circ$ ,  $\beta = 60^\circ$ ) during uniaxial loading. The denoted letter shown in the figure is corresponding to Fig. 13

to those in Fig. 13. From Figs. 13-14, we can see that the crack evolution process of sandstone specimen containing combined flaws ( $\alpha = 60^\circ$ ,  $\beta = 60^\circ$ ) was very approximate to that for  $\alpha = 30^\circ$  and  $\beta = 60^\circ$ .

In accordance with Figs. 13-14, it can be seen when the axial stress is loaded to point a, the specimen begins to initiate tensile crack 1 at the upper and under tip of fissure, the top and bottom edge of two squares. The initiation of tensile crack 1 leads to a minor stress drop. Afterwards, as the deformation progressed, the length of crack from the top and bottom edge of two squares begins to propagate towards the end surface of the specimen along the direction of major principal stress. But the tensile crack 1<sup>a</sup>, 1<sup>c</sup>-1<sup>d</sup>, and 1<sup>f</sup> did not propagate a lot, which was due to the stress concentration field between fissure and double squares. When the specimen is loaded to point e ( $\sigma_1 = 53.74 \text{ MPa} = 99.7\% \sigma_c$ ) after the peak strength, tensile crack 2<sup>a</sup> merges rapidly between the upper tip of fissure and the left middle side part of square ①, and tensile crack 2<sup>b</sup> between the under tip of fissure and the right top corner of square ②. The coalescence of tensile crack 2 also leads to an obvious stress drop from 53.74 to 37.13 MPa like the specimen for  $\alpha = 30^\circ$ . After the stress drop at point e, the continuous increase of axial deformation leads to that the axial stress of the specimen begins to increase slowly with a lower deformation modulus than that before point e, which results from some minor damages of the supporting structure in the specimen (Fig. 14(e)). When the specimen is loaded to point g, the axial stress-strain curve begins to depart from the linearity because of hole collapse of two squares. It should be noted that in the deformation process from point h to point i, even though the axial strain continues to increase, the axial stress keeps basically a constant, which can be seen from local magnification shown in Fig. 13. Hole collapse of two squares in the specimen is a gradual evolution process, as shown in Fig. 15. After point h, the specimen takes place the unstable failure.

#### 4. Conclusions

In this paper, by using rock mechanics servo-controlled testing system and photographic monitoring technique, uniaxial compression experiment are carried out for brittle sandstone specimen containing pre-existing different flaws to analyze its deformation behaviour and crack evolution process. Based on the experimental results, the following conclusions can be drawn.

- (1) The crack initiation stress, uniaxial compressive strength and peak axial strain of specimen containing a single fissure are all higher than those containing double squares, while which are higher than those containing combined flaws. For sandstone specimen containing combined flaws, the uniaxial compressive strength of sandstone increase as the  $\alpha$  increases from  $30^\circ$  to  $90^\circ$ , which indicates that the specimens with steeper fissure angles can support higher axial capacity for  $\alpha$  greater than  $30^\circ$ . However, the crack initiation stress of sandstone specimen containing combined flaws is not dependent obviously to fissure angle for  $\alpha$  greater than  $30^\circ$ .
- (2) The crack evolution process of brittle sandstone specimens containing a single fissure, double squares and combined flaws are analyzed detailed by photographic monitoring technique. For the specimen containing a single fissure, tensile wing cracks are first initiated at the upper and under tips of fissure, and anti-tensile cracks and far-field cracks are also observed in the deformation process; moreover anti-tensile cracks usually accompanies with tensile wing cracks. For the specimen containing double squares, tensile cracks are usually initiated from the top and bottom edge of two squares along the direction of axial stress, and in the process of final unstable failure, more vertical splitting failures are observed in the ligament region.
- (3) When a single fissure and double squares are formed together into combined flaws, the crack evolution process is different from that containing a single fissure or double squares. Even though initiated at the upper and under tip of fissure, tensile wing cracks do not propagate to the end surface of the specimen like that in the specimen containing a single fissure. The crack coalescence between the fissure tips and double squares plays a significant role for ultimate failure of the specimen containing combined flaws.

## Acknowledgments

This research was supported by the National Basic Research 973 Program of China (Grant No. 2014CB046905), the Fundamental Research Funds for the Central Universities (China University of Mining and Technology) (Grant No. 2014YC10), for which the authors are very grateful. The author would also like to express his sincere gratitude to the editor and the anonymous reviewers for their valuable comments, which have greatly improved this paper.

## References

- Debecker, B. and Vervoort, A. (2009), "Experimental observation of fracture patterns in layered slate", *Int. J. Fract.*, **159**(1), 51-62.
- Feng, X.T., Ding, W.X. and Zhang, D.X. (2009), "Multi-crack interaction in limestone subject to stress and flow of chemical solutions", *Int. J. Rock Mech. Min. Sci.*, **46**(1), 159-171.
- Hall, S.A., Sanctis, F. and Viggiani, G. (2006), "Monitoring fracture propagation in a soft rock (Neapolitan Tuff) using acoustic emissions and digital images", *Pure Appl. Geophys.*, **163**(10), 2171-2204.
- Janeiro, R.P. and Einstein, H.H. (2010), "Experimental study of the cracking behaviour of specimens containing inclusions (under uniaxial compression)", *Int. J. Fract.*, **164**(1), 83-102.
- Lee, H. and Jeon, S. (2011), "An experimental and numerical study of fracture coalescence in pre-cracked specimens under uniaxial compression", *Int. J. Solids Struct.*, **48**(6), 979-999.
- Li, Y.P., Chen, L.Z. and Wang, Y.H. (2005), "Experimental research on pre-cracked marble under

- compression”, *Int. J. Solids Struct.*, **42**(9-10), 2505-2516.
- Park, C.H. and Bobet, A. (2009), “Crack coalescence in specimens with open and closed flaws: A comparison”, *Int. J. Rock Mech. Min. Sci.*, **46**(5), 819-829.
- Prudencio, M. and Van Sint Jan, M. (2007), “Strength and failure modes of rock mass models with non-persistent joints”, *Int. J. Rock Mech. Min. Sci.*, **44**(6), 890-902.
- Wong, L.N.Y. and Einstein, H.H. (2009), “Crack coalescence in molded gypsum and Carrara marble: Part I: Macroscopic observations”, *Rock Mech. Rock Eng.*, **42**(3), 475-511.
- Yang, S.Q. and Jing, H.W. (2011), “Strength failure and crack coalescence behavior of brittle sandstone samples containing a single fissure under uniaxial compression”, *Int. J. Fract.*, **168**(2), 227-250.
- Yang, S.Q., Yang, D.S., Jing, H.W., Li, Y.H. and Wang, S.Y. (2012), “An experimental study of the fracture coalescence behaviour of brittle sandstone specimens containing three fissures”, *Rock Mech. Rock Eng.*, **45**(4), 563-582.
- Yang, S.Q., Liu, X.R. and Jing, H.W. (2013), “Experimental investigation on fracture coalescence behavior of red sandstone containing two unparallel fissures under uniaxial compression”, *Int. J. Rock Mech. Min. Sci.*, **63**, 82-92.
- Yin, P., Wong, R.H.C. and Chau, K.T. (2014), “Coalescence of two parallel pre-existing surface cracks in granite”, *Int. J. Rock Mech. Min. Sci.*, **68**, 66-84.